Laminar entrance flow in curved annular ducts

Hoon Ki Choi* and Seung O. Park†
Department of Mechanical Engineering* and Department of Aerospace Engineering,†
Korea Advanced Institute of Science and Technology, Yusung-ku, Taejon, Korea

Steady laminar flows in coiled annular ducts are investigated numerically. Numerical solutions are obtained by solving the incompressible Navier-Stokes equation with a SIMPLE type procedure for annular curved ducts of various radius ratio for a given Reynolds number. Effect of radius ratio on the flow development is given particular attention. Computational results indicate that the secondary flow in a half cross section (above or below the line of symmetry) for the case of moderate radius ratio is characterized by a pair of counter-rotating vortices; the flow in the core region is toward the outside bend and the flow near the inner and outer walls is toward the inside bend. However, when the radius ratio is very large, say greater than 0.8, the secondary flow is unidirectional and is toward the inside bend, owing to the strong viscous effect. It is also found that the downstream flow development is greatly affected by the radius ratio. When the radius ratio is moderate, the centroid of the first moment of streamwise velocity lies on the outside half plane; when the radius ratio is very large, the centroid lies on the inside half plane. In contrast to the case of straight annular duct, the flow in a curved annular duct is not necessarily fully developed earlier when the radius ratio is larger owing to the complicated interaction between the viscous and the centrifugal forces.

Keywords: laminar flow; internal flow; curved annulus; secondary flow

Introduction

Internal flows in curved ducts of various cross-sectional shapes form an important class of engineering flows. Particularly, fluid flow in curved pipes has attracted considerable attention because of its wide range of applications, e.g., in heat exchangers and piping systems. Fully developed and developing flows in curved pipes have been studied by many investigators as reviewed in Berger et al.[1] Studies about the flow in a curved annulus, however, are few. It is expected that the flow in a curved annulus will be significantly different from that in a curved pipe because of the presence of an inner pipe around which an additional inner wall boundary layer has to be established. It is known that secondary flows in curved flow passages originate principally from the interaction between the centrifugal force, the pressure gradient, and the viscous forces. Thus, the secondary flow features in a curved annulus will be very different from those in a curved pipe because of the additional inner wall boundary layer in the former. Further, the importance of the inner and outer wall boundary layers will be influenced by the extent of the annular region usually represented by the radius ratio.

The purpose of the present study is to examine the flow details of developing laminar flow in several curved annuli having different radius ratios for a given Reynolds number. The effect of radius ratio on the flow in straight annular ducts has been investigated by several authors.[2–4] Lundgren et al.[2] and Sparrow and Lin[3] showed that the pressure drop in the entrance region of an annular duct was very similar to that in parallel-plate channel over a wide range of radius ratio, say, from 0.3 to approximately 1.0. However, the pressure drop for the case of a very small radius ratio, say, below 0.001, significantly departed from that for a straight circular pipe. Sparrow and Lin[3] and McComas[4] found that the entrance length in terms of hydraulic radius increased with the decrease of the radius ratio. The entrance length would be shortened considerably if the radius of the inner tube became larger. Humphrey[5] obtained numerical solutions for developing laminar flow in curved annuli having 90° bend. He found that the secondary flow comprised two pairs of cross-stream vortices owing to the presence of the inner curved wall. He concentrated on the flow in the curved annuli of the radius ratio of 0.3 and 0.6, and thus the effect of very large radius ratio on the flow development was not addressed in his work. Recently, Garimella et al.[6] studied experimentally the forced convection heat transfer in coiled annular ducts. In that study, however, only average heat transfer coefficients were investigated and thus detailed flow features were lacking.

In the present study, the full Navier-Stokes equation was solved for coiled annular ducts of varying radius ratio for a given Reynolds number. The Reynolds number was set at 800 and the radius ratio was varied from 0.2–0.9. This corresponds to the Dean number range of approximately 220–640 when the following definition of Dean number is employed.

$$\kappa = 2\,\mathrm{Re}\,\delta_h^{1/2} \tag{1}$$

where Re is the Reynolds number based on hydraulic radius and δ_h is the ratio of the hydraulic radius of the annulus to the

Address reprint requests to Dr. Park at the Dept. of Aerospace Engineering, Korea Advanced Institute of Science and Technology, 373-1 Kusong-Dong, Yusung-ku, Taejon, Korea.

Received 1 October 1990; accepted 27 August 1991

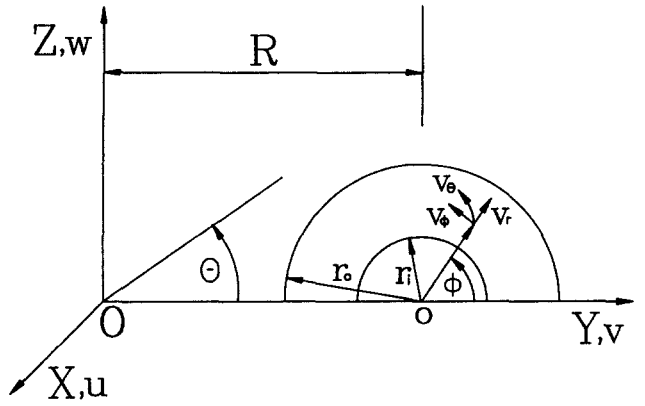

Figure 1 Schematic of the flow field and toroidal coordinate system

radius of curvature of the coil. The coordinate system for the present problem is sketched in Figure 1. Several essential features about the flow in curved annuli were found by Humphrey.[5] However, his computations were performed mainly for the curved annuli of small radius ratios on a rather coarse grid and the computational domain was rather narrow; the outflow boundary was set at the azimuthal angle (streamwise direction) of 90°. The present computations were carried out on a much denser grid over a larger computational domain covering the flows of a wider range of radius ratio. Thus, it is anticipated that the results of the present study will add to the current knowledge about the curved annular duct flow, including the effect of the radius ratio on the flow development.

Numerical details

Outline of the solution procedure

To obtain numerical solutions for the present problem, we adopted and modified the three-dimensional incompressible Navier-Stokes solver developed by Chen.[7] Since the full details of the numerical scheme and computational procedures are available elsewhere,[7] only a brief sketch of the solution method is described below. The governing equations for steady, constant property flow in flux vector form can be written as

$$E_x + F_y + G_z = S \tag{2}$$

where

$$E = \begin{bmatrix} \rho u \\ \rho uu - \mu u_x \\ \rho uv - \mu v_x \\ \rho uw - \mu w_x \end{bmatrix}, \quad F = \begin{bmatrix} \rho v \\ \rho vu - \mu u_y \\ \rho vv - \mu v_y \\ \rho vw - \mu w_y \end{bmatrix},$$

$$G = \begin{bmatrix} \rho w \\ \rho wu - \mu u_z \\ \rho wv - \mu v_z \\ \rho ww - \mu w_z \end{bmatrix}, \quad S = \begin{bmatrix} 0 \\ -p_x \\ -p_y \\ -p_z \end{bmatrix}$$

When Equation 2 is transformed into a general curvilinear coordinate system (ξ, η, ζ), it becomes

$$E_\xi \xi_x + E_\eta \eta_x + E_\zeta \zeta_x + F_\xi \xi_y + F_\eta \eta_y + F_\zeta \zeta_y + G_\xi \xi_z + G_\eta \eta_z + G_\zeta \zeta_z = S \tag{3}$$

The Jacobian of the transformation and the relationships among the derivatives ξ_x, ξ_y, ξ_z, η_x, η_y, η_z, ζ_x, ζ_y, ζ_z, and the derivatives x_ξ, x_η, x_ζ, y_ξ, y_η, y_ζ, z_ξ, z_η, and z_ζ are the same as those given in the textbook by Hoffmann.[8] For the present problem, the x-, y-, and z-coordinates of the physical space are specified from the relation between the Cartesian and the toroidal coordinate system. With the given x, y, and z values, grid transformation coefficients and the Jacobian of the transformation are numerically evaluated. It is noted that we employ a general curvilinear coordinate system for the computation, whereas Humphrey[5] used the governing equations in the toroidal coordinate system and the corresponding discretized equations. Equation 3 is integrated over the control volume formed by the incremental length $\Delta\xi$, $\Delta\eta$, and $\Delta\zeta$, which are unity, respectively. For the integration, a staggered grid system used by Vanka et al.[9] is adopted. The second-order central differencing for the diffusion terms and the hybrid scheme[10] for the convection terms are employed in the present work. The discretized equation finally takes the form

$$A_P\phi_P = A_E\phi_E + A_W\phi_W + A_N\phi_N + A_S\phi_S + A_T\phi_T + A_B\phi_B + S_C \tag{4}$$

The coefficient A_P is given by

$$A_P = A_E + A_W + A_N + A_S + A_T + A_B - S_P \tag{5}$$

where A_E, A_W, A_N, A_S, A_T, and A_B are the link coefficients that can be found easily.[10]

To solve for the pressure field, we adopt the pressure correction procedure employed in SIMPLE-C algorithm.[11] The pressure correction procedure of SIMPLE-C is known to be more consistent than that of SIMPLE. The final pressure

Notation

A	Cross-sectional area $= \pi(r_o^2 - r_i^2)$
C_p	Pressure coefficient $= \dfrac{p - p_{ref}}{\frac{1}{2}\rho U^2}$
R	Radius of curvature of the bend
Re	Reynolds number based on hydraulic radius $= r_h U/\nu$
r_i	Inner radius of annulus
r_o	Outer radius of annulus
r_h	Hydraulic radius $= 2A/S$
S	Wetter perimeter $= 2\pi(r_o + r_i)$
U	Nondimensional streamwise velocity
u, v, w	x-, y-, and z-components of the nondimensional velocities
x, y, z	Nondimensional Cartesian coordinates
v_r, v_ϕ, v_θ	r, ϕ, and θ components of the nondimensional velocities
r, ϕ, θ	Nondimensional toroidal coordinates

Greek symbols

α	Radius ratio $= r_i/r_o$
δ_h	Curvature ratio based on hydraulic radius $= r_h/R$
ν	Kinematic viscosity
κ	Dean number $= 2\,\mathrm{Re}\,\delta_h^{1/2}$

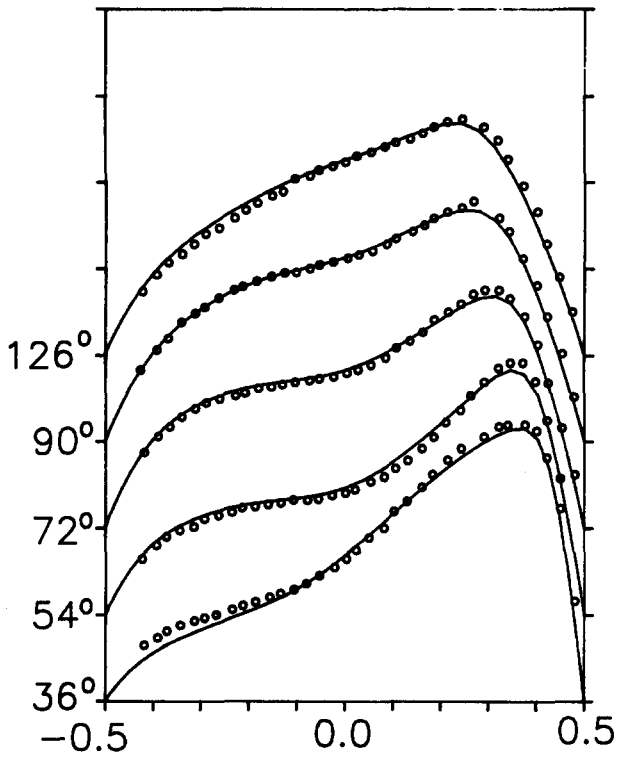

Figure 2 Developing streamwise velocity profiles on the plane of symmetry of a curved square duct for $\kappa = 226$, Re = 574. ———, Present calculation; ○, Hille et al

correction equation, however, also takes the form given by Equation 4. Equation 4 is solved iteratively by a line under relaxation procedure until the solution achieves a desired accuracy.

Code verification

To ensure that the present code works properly, we carried out computations for two laminar curved duct flows: one with a square cross section and the other with a circular cross section. The curved square duct flow studied experimentally by Hille and Vehrenkamp[12] and the curved circular pipe flow investigated experimentally by Agrawal et al.[13] and numerically by Soh and Berger[14] were chosen as the two test flows to validate the present code.

Figure 2 compares the predicted streamwise velocity profiles with those of the experimental data of Hille and Vehrenkamp.[12] The computation was done on a 35 * 35 (cross section) * 99 (streamwise direction) mesh. The computational inlet plane was located at about 5.3 hydraulic diameters upstream on the straight section from the curved duct inlet. Fully developed velocity profile was specified at the inlet plane. The exit plane of the computational domain was set at 14 hydraulic diameters downstream on the straight section extending from the end of the 180° curved bend, and fully developed conditions were specified at the exit plane.

In Figure 3, the predicted velocity profiles for the curved pipe flow were compared with those of Agrawal et al.[13] and with the numerical results of Soh and Berger.[14] The calculation was performed on a 31 * 31 (cross section) * 109 (streamwise direction) mesh. At the inlet of the curved pipe, the velocity profiles given by Soh and Berger[14] were specified. Fully developed conditions were given at the exit plane located at $\theta = 3\pi/2$.

The results of computation with the present code contained in Figures 2 and 3 clearly show that the numerical scheme adopted in the present study works properly.

Boundary conditions

The boundary conditions for the present problem of curved annular flow are discussed in this section. Since Equation 3 is elliptic, boundary conditions have to be imposed for all of the boundary surfaces. The fluid-flow boundaries for the present problem are composed of four regions: the inlet cross section, the rigid walls surrounding the fluid, the plane of symmetry, and the far downstream cross section.

At the inlet plane, uniform streamwise velocity was specified for most of the calculations in the present work. In practice, uniform inlet flow condition can hardly be realized. In our judgement, however, the effect of radius ratio on the flow development could be assessed successfully by specifying the uniform inlet flow condition, which was a prime motivation for the present study. To investigate the significance of the inlet flow condition, a straight annular duct was deliberately attached to the inlet of the annular coil so that a parabolic flow condition was established at the inlet plane of the coil. In this case, we specified the fully developed velocity profile at the inlet of the straight annulus. The results of such treatment are discussed later.

The no-slip condition was applied at the inner and outer wall surfaces. At the plane of symmetry, the following symmetry condition was imposed.

$$\frac{\partial v_r}{\partial \phi} = \frac{\partial v_\theta}{\partial \phi} = 0, \qquad v_\phi = 0 \tag{6}$$

A review of the published results on the flow in curved ducts of various cross-sectional shape showed that the symmetry

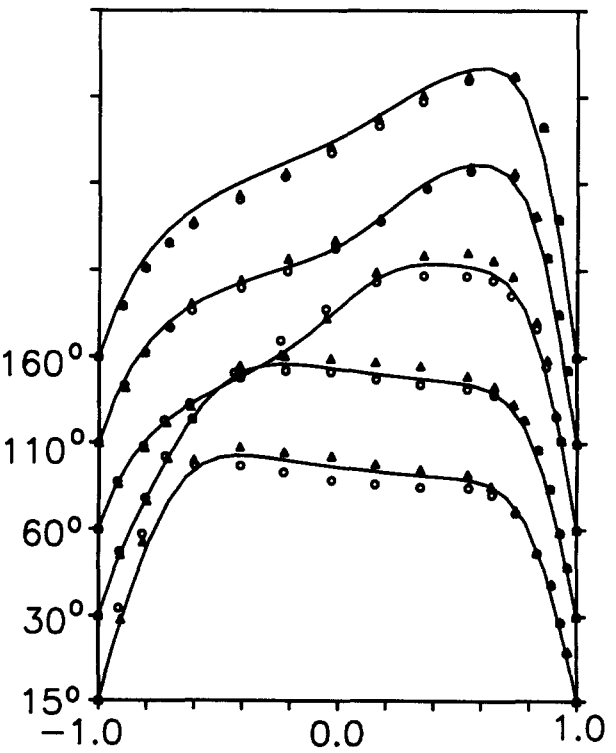

Figure 3 Developing streamwise velocity profiles on the plane of symmetry of a curved circular pipe for $\kappa = 183$, Re = 242. ———, Present calculation; ○, Soh and Berger; Δ, Agrawal et al

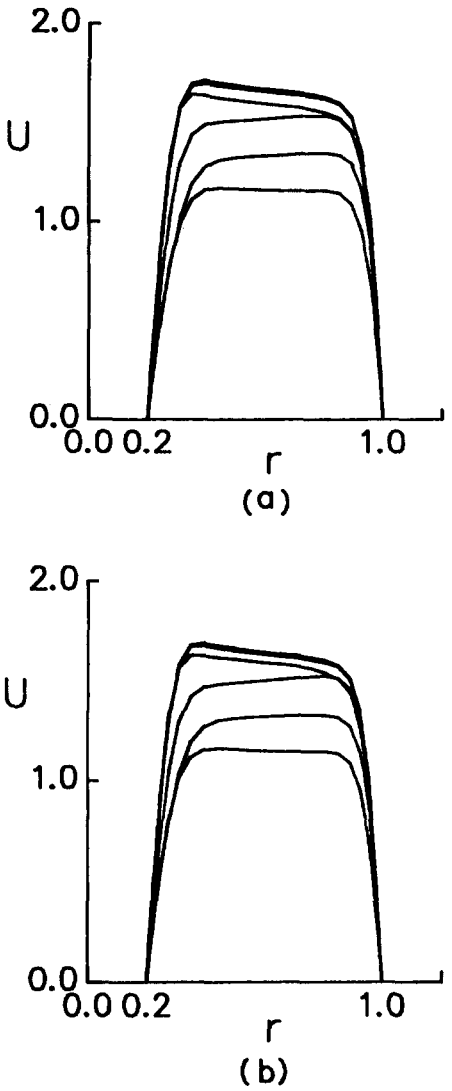

Figure 4 Plots of the streamwise velocity profile for $\alpha = 0.2$, $\kappa = 640$ ($\phi = 0°$): (1) $\theta = 18°$; (2) $\theta = 72°$; (3) $\theta = 144°$; (4) $\theta = 234°$; (5) $\theta = 302°$; (6) $\theta = 324°$. The exit boundary specified (a) at $\theta = 360°$; (b) $\theta = 396°$

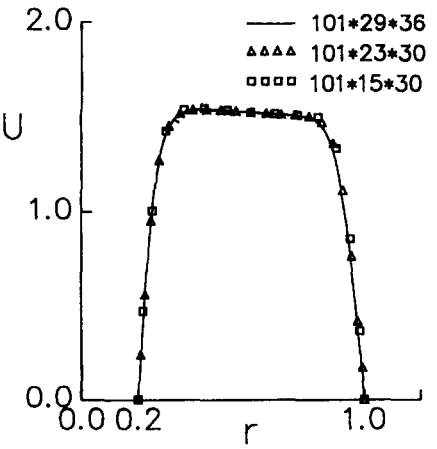

Figure 5 Grid effects on the streamwise velocity profile for $\alpha = 0.2$, $\kappa = 640$ ($\phi = 0°$, $\theta = 180°$)

condition did not hold for some cases. For example, Hille and Vehrenkamp[12] and Humphrey et al.[15] showed that the flow motion in a curved rectangular duct was asymmetric when the Dean number was relatively high. For the flows in curved circular pipes studied by Olson and Snyder,[16] Futagami,[17] and Prusa and Yao,[18] we found that the flows were symmetric. The Dean number for these cases ranged from 12–660. In fact, the symmetry condition was used for most of the computational studies on curved pipe flows.[18–21] For annular flow, Humphrey[5] adopted the symmetry condition of Equation 6. The critical Dean number above which the curved annular flow becomes asymmetric is not yet available. However, because the Dean number for the present work was not high, we conjectured that the symmetry condition given as above should be satisfactory. The work on the asymmetric flow motion and the corresponding critical Dean number for curved annular duct flow is left for future effort.

We assumed that the streamwise derivatives of all the velocity components vanish far downstream, which is expressed as

$$\frac{\partial v_r}{\partial \theta} = \frac{\partial v_\phi}{\partial \theta} = \frac{\partial v_\theta}{\partial \theta} = 0 \tag{7}$$

In the present work, the streamwise variable $\theta = 360°$ was taken as far downstream. The choice of far downstream was considered to be sufficient in view of the fact that the far downstream for coiled pipes rarely exceeded $\theta = 270°$ (e.g., see Soh and Berger[14]). In Humphrey's[5] work on annular duct flow, he took $\theta = 90°$ as exit boundary. The reader is reminded that the entrance length for straight annular ducts is shorter than that for straight pipes. We thus concluded that $\theta = 360°$ could well be taken as the exit boundary. To support the above choice of the exit boundary, we also performed the computation with the exit boundary condition specified at $\theta = 396°$. The sensitivity of streamwise velocity distribution on the exit boundary is shown in Figure 4. Figure 4 clearly shows that the specification of the exit boundary condition at $\theta = 360°$ is indeed sufficient. The streamwise velocity profiles shown in Figure 4 are all nearly the same. We also note that the streamwise velocity profile has reached a fully developed state at about $\theta = 300°$.

Grid system and convergence criteria

We distributed 15–23 grid points radially depending on the radius ratio for the present computation. The grid points were stretched unevenly to put more points in the viscous wall region. Thirty and 101 grid points were distributed evenly in the circumferential and the streamwise direction, respectively. As an attempt to examine the grid dependence of the solution, we also carried out the calculation on three different grid systems for the case of $\alpha = 0.2$. The results are shown in Figure 5. As can be seen, the discrepancy between the solutions is minute.

The solution was taken as converged when the following criterion was met.

$$(|\Delta u|_{max} + |\Delta v|_{max} + |\Delta w|_{max})/U_{ref} + |p'|_{max}/\rho U_{ref}^2 \leqslant 10^{-4} \tag{8}$$

where Δu, Δv, Δw, and p' represent velocity changes and pressure correction value during each iteration.

Results and discussion

Secondary flow development

Figures 6 and 7 display the development of secondary flow for the annular ducts of $\alpha = 0.2$ and 0.5, respectively. For both

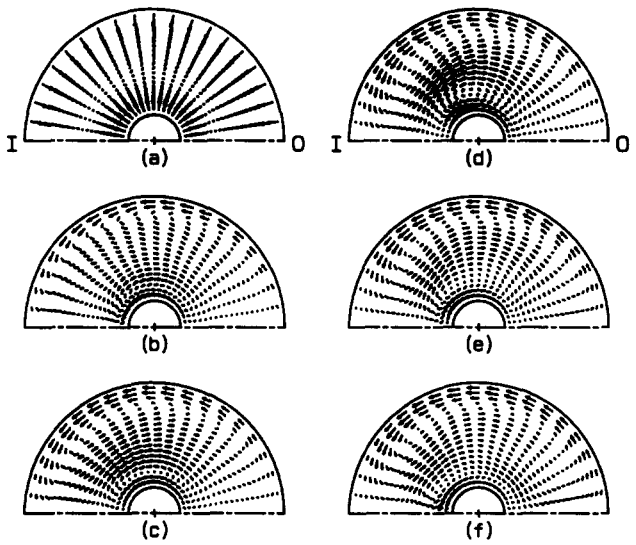

Figure 6 Vector plot of the secondary flow for $\alpha = 0.2$, $\kappa = 640$: (a) $\theta = 3.6°$, $v_\phi)^{max} = 0.06$; (b) $\theta = 25.2°$, $v_\phi)_{max} = 0.12$; (c) $\theta = 61.2°$, $v_\phi)_{max} = 0.28$; (d) $\theta = 108°$, $v_\phi)_{max} = 0.35$; (e) $\theta = 180°$, $v_\phi)_{max} = 0.32$; (f) $\theta = 252°$, $v_\phi)_{max} = 0.32$

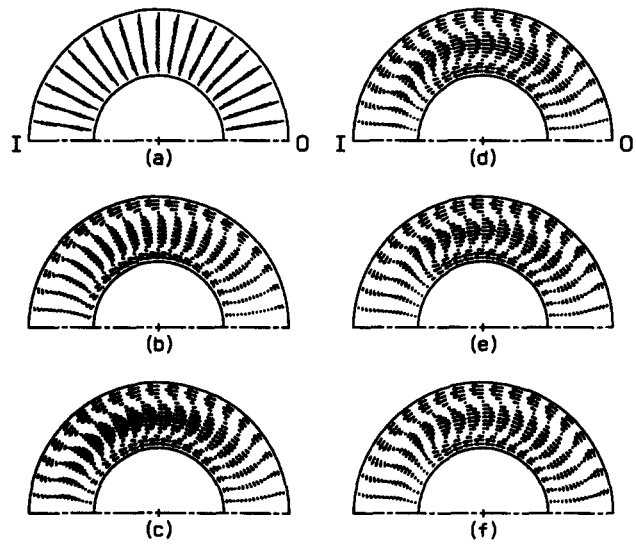

Figure 7 Vector plot of the secondary flow for $\alpha = 0.5$, $\kappa = 506$: (a) $\theta = 3.6°$, $v_\phi)_{max} = 0.06$; (b) $\theta = 25.2°$, $v_\phi)_{max} = 0.10$; (c) $\theta = 61.2°$, $v_\phi)_{max} = 0.22$; (d) $\theta = 108°$, $v_\phi)_{max} = 0.32$; (e) $\theta = 180°$, $v_\phi)_{max} = 0.29$; (f) $\theta = 252°$, $v_\phi)_{max} = 0.28$

cases, the flow starts from the uniform streamwise velocity inlet condition. As the boundary layers grow from the inner and outer walls, the fluid moves toward the central core region. The cross-stream velocity at this stage is core-ward (Figures 6a and 7a). The situation is essentially the same as that of the developing flow near the inlet in a straight annular duct where the cross-stream flow is also directed to the core region. This suggests that the influence of the centrifugal force is not immediately felt near the inlet when the flow starts from the uniform velocity condition. However, the circumstance changes very much when the flow is first developed through a straight annulus and then enters the coiled section. The secondary flow pattern at the inlet plane of the coiled section (i.e., $\theta = 0°$) for this case is shown in Figure 8. Clearly, the secondary motion is directed to the inside of the bend of the coil, contrary to the case of uniform velocity condition where the initial secondary motion is core-ward. As the fluid enters the curved section, the fluid near the inside portion of the bend can travel further without obstruction (i.e., the wall boundary) than that near the outside portion of the bend because of the curved geometry. Thus, the inside fluid drags the outside fluid to result in the inward secondary motion seen in Figure 8. The cause of secondary motion for this case is therefore somewhat different from the viscous nature of those seen in Figures 6a and 7a. The inertia of the entering fluid is the primary cause of the inward flow for this case. A similar inward secondary motion at the inlet plane of the curved section for a curved square duct and a curved circular pipe has been observed experimentally by Humphrey et al.[15] and Bovendeerd et al.,[22] respectively. It is commented here that the flow in this case is elliptic in nature as opposed to the general convention that the flow in a constant area duct is usually parabolic. Perhaps, if a once-through parabolic calculation procedure were employed for the present calculation, the inward secondary flow due to inertial effect seen in Figure 8 might not have been captured. As will be discussed later, the eventual secondary flow pattern, however, is not likely to be altered by the inlet flow condition. Thus, we continue our discussion based on the computational results obtained using uniform inlet flow condition.

As the flow proceeds farther downstream from the inlet, the centrifugal force begins to take effect in establishing secondary motion, as seen in Figures 6 and 7. Pressure gradient parallel to the line of symmetry is essentially determined by the centrifugal force due to the streamwise velocity and the curvature of the bend. Further, the pressure is nearly uniform along lines normal to the line of symmetry. Since the streamwise velocity near the wall is much smaller than that in the core region because of the no-slip condition, the slower moving fluid particles near the wall region have to move inward (i.e., in the direction of decreasing radius of curvature) to maintain the momentum balance between the centrifugal force and the pressure gradient. This leads to the onset of secondary flow such that the fluid particles near the upper and the lower walls move inward while those in the core region move outward, as shown in Figures 6 and 7. The presence of the upper and lower wall normally makes the secondary flow two-celled (counter-rotating pair of vortices), contrary to the one-cell pattern common in curved pipe flows. This supports the previous finding of Humphrey[5] that the flow in curved annuli had a pair of cross-stream vortices in a half plane. It is noticeable that the circumferential velocity near the upper wall is considerably greater than that near the lower wall, reflecting the fact that

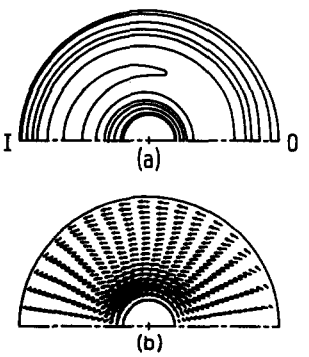

Figure 8 Plots of the streamwise isovelocity contours; (a) vector plot of the secondary flow $(v_\phi)_{max} = 0.11$); (b) $\theta = 0°$ for $\alpha = 0.2$, $\kappa = 640$ (flow starts from a straight duct and then enters the curved section)

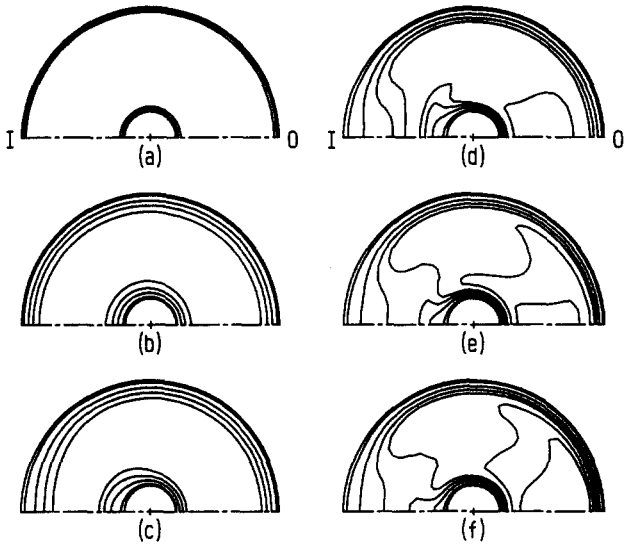

Figure 9 Plots of the streamwise isovelocity contours for $\alpha = 0.2$, $\kappa = 640$: (a) $\theta = 3.6°$; (b) $\theta = 25.2°$; (c) $\theta = 61.2°$; (d) $\theta = 108°$; (e) $\theta = 180°$; (f) $\theta = 252°$

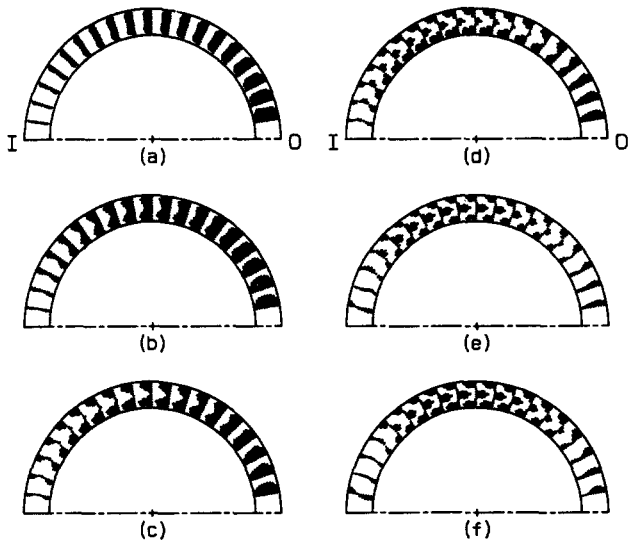

Figure 10 Vector plot of the secondary flow for $\alpha = 0.8$, $\kappa = 320$: (a) $\theta = 7.2°$, $v_\phi)_{max} = 0.14$; (b) $\theta = 25.2°$, $v_\phi)_{max} = 0.16$; (c) $\theta = 72°$, $v_\phi)_{max} = 0.16$; (d) $\theta = 144°$, $v_\phi)_{max} = 0.20$; (e) $\theta = 252°$, $v_\phi)_{max} = 0.35$; (f) $\theta = 320.4°$, $v_\phi)_{max} = 0.38$

the pressure gradient (along the line of symmetry) experienced by the fluid particles in the upper wall region is much larger than in the lower wall region.

Several interesting observations can be made when we compare Figures 6 and 7. The magnitude of the circumferential velocity near the inside bend wall boundary becomes larger when the radius of the inner pipe increases since the circumferential pressure gradient felt by the fluid particles adjacent to the boundary gets stronger with the length of the wall boundary. This makes the strength of the lower cell vortex increase with the decrease of the radius ratio. We also find that the position of the two vortex centers (lower and upper cell vortices) depends heavily on the radius ratio. For the flow of $\alpha = 0.2$ (Figure 6), the two vortex centers are seen to be located far off centerline ($\phi = 90°$ line); for the flow of $\alpha = 0.5$ (Figure 7), the two centers are located about the centerline.

The flow development process is also greatly affected by the radius ratio. The secondary flow patterns contained in Figure 6 illustrate that the upper vortical cell has essentially reached a fully developed stage at about $\theta = 108°$. On the contrary, the lower vortical cell develops further. For example, the center of the lower-cell vortex shifts inward as the flow progresses (Figures 6d, e, and f). Iso-streamwise velocity lines depicted in Figure 9 also confirm the observation described previously. For the case of a larger radius ratio (Figure 7), both the upper and the lower cell are essentially fully developed at about $\theta = 108°$.

A more interesting case of flow development for $\alpha = 0.8$ is illustrated in Figure 10. In contrast to the two previous cases, the centrifugal motion (i.e., an outward motion in the central core region) has not yet been effected at $\theta = 25.2°$. Owing to the inward motion at the initial stage, the streamwise velocity around the inside bend increases. This results in an increase of centrifugal force to overcome the opposing pressure gradient, and hence the outward centrifugal motion in the core region starts to appear around the inside bend, as seen in Figure 10c. As the flow progresses farther downstream, the outward centrifugal motion gets stronger and the inward motion is confined within the near wall regions. The flow keeps developing as far as $\theta = 320.4°$, as can be noted in Figures 10e and f. The dominance of inward motion over the whole width of the duct up to a considerable downstream distance is a characteristic feature of the flow of large α. This can be made clearer when we examine the cross-stream velocity vectors for the case of $\alpha = 0.9$ (Figure 11). The inward motion persists as far as $\theta = 46.8°$. Even at $\theta = 144°$ the inward motion still prevails except for the region close to $\phi = 180°$, where a very weak outward centrifugal motion may be noticed. The occurrence of outward centrifugal motion is very much inhibited by the strong viscous action. The streamwise velocity in this case can hardly be increased because of the narrow gap. The two vortical cells conspicuous in Figures 6 and 7 are not distinguishable in Figures 10 and 11. For the flows of large radius ratio, the notion of vortical cell seems to become very ambiguous and is therefore not adequate in describing the secondary flow.

Evidently, the position where the centrifugal motion starts to appear is strongly dependent on the radius ratio. When the radius ratio is large, the viscous effect dominates the flow development and thus the appearance of the outward centrifugal motion is delayed. We comment here that the larger radius ratio is equivalent to the smaller Dean number in the

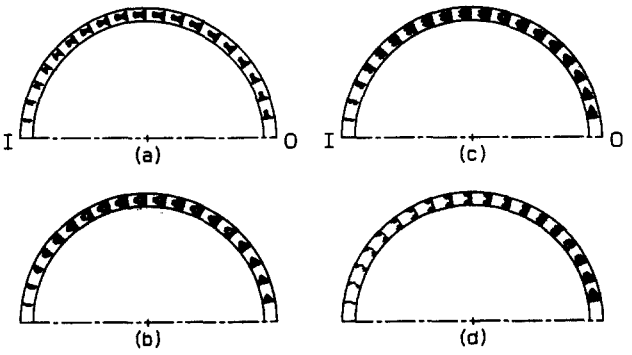

Figure 11 Vector plot of the secondary flow for $\alpha = 0.9$, $\kappa = 226$: (a) $\theta = 3.6°$, $v_\phi)_{max} = 0.07$; (b) $\theta = 18°$, $v_\phi)_{max} = 0.10$; (c) $\theta = 46.8°$, $v_\phi)_{max} = 0.06$; (d) $\theta = 126°$, $v_\phi)_{max} = 0.06$

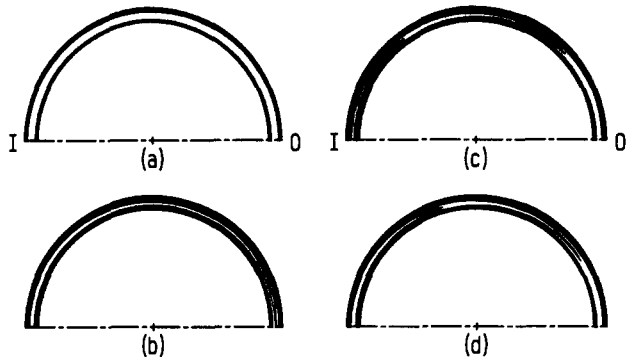

Figure 12 Plots of the streamwise isovelocity contours for $\alpha = 0.9$, $\kappa = 226$: (a) $\theta = 3.6°$; (b) $\theta = 18°$; (c) $\theta = 46.8°$; (d) $\theta = 126°$

present study. The smaller Dean number thus implies the importance of the inward motion in the present cases, which is qualitatively similar to the case of curved pipe flows. In curved pipe flows, it is known that the center of the vortex moves to the outside bend as the Dean number increases. To draw a similar conclusion, however, we would need a series of computations for a fixed radius ratio over a wide range of the Dean number, which is left for future work. It is well established that the flow is fully developed earlier when the radius ratio is larger for straight annular ducts. For the curved annular flows, however, the situation becomes more complex owing to the interaction between the centrifugal and viscous forces. As evidenced from the case of $\alpha = 0.8$, the flow can hardly be said to be fully developed even at $\theta = 252°$. For the cases of $\alpha = 0.2$ and 0.5, however, the flows may be said to be fully developed at $\theta = 252°$.

Streamwise velocity development

The development of iso-streamwise velocity contours illustrated in Figure 9 shows that the growth of the wall boundary layers at the initial stage of turning is principally governed by the viscous effect. The iso-velocity lines in Figures 9a and b are approximately equally spaced for the entire region, implying that the centrifugal force has at most negligible effect. At $\theta = 61.2°$, we clearly see that the boundary layer along the inside bend has grown thicker owing to the migration of the boundary-layer fluid particles toward the inside bend. The equally spaced nature of iso-streamwise velocity lines (hence, the dominance of viscous effect) is noticeable throughout the contour plots shown in Figure 12.

A shift of streamwise momentum about the center of the annulus can conveniently be represented by the first moment of the streamwise velocity suggested by Olson and Snyder.[16]

$$M_o = \frac{\int_o^{\pi}\int_{r_i}^{r_o} \frac{v_\theta x}{r_o}\, r\, dr\, d\phi}{\int_o^{\pi}\int_{r_i}^{r_o} v_\theta r\, dr\, d\phi} \tag{9}$$

where x is the Cartesian coordinate with the origin located at the center of the annular cross section. Thus, if the streamwise velocity is uniform over the whole cross section, M_o will be zero. If the average streamwise velocity over the inside half of the bend is greater than that over the outside half, M_o will be negative and vice versa. Figure 13 shows the change of M_o with downstream for various flow conditions. We first note that M_o is greatly influenced by the radius ratio. For the cases of $\alpha = 0.2$ and 0.5, the first moment M_o becomes positive as the flow develops downstream owing to strong outward centrifugal motion. When $\alpha = 0.9$, M_o becomes negative, contrary to the cases of smaller radius ratio. The negative value of M_o, which signifies that the streamwise velocity in the inside bend is generally greater than that in the outside bend, results from the inward motion, as already depicted in Figure 11. This again confirms that the outward centrifugal motion is rather insignificant when the radius ratio is very large. The shift of the first moment for $\alpha = 0.8$ deserves particular attention. When the flow proceeds downstream, the center of the first moment shifts to the inside bend (negative M_o) owing to the inward motion. Then, at the late stage of development, the negative shift gradually tends toward the center of the annulus as the outward centrifugal motion becomes effective. It is interesting to note that the centroid of the first moment at the final stage is located about the center of the annulus, suggesting that the momentum shift due to inward motion and that due to outward centrifugal motion are in approximate balance.

We have seen that the secondary flow development at the initial stage (i.e., near the inlet of the curved bend) is dictated by the inertial effect (Figure 8). The inertial effect on the first moment for $\alpha = 0.2$ is shown by the solid line of Figure 13. The solid line represents the shift of first moment when the flow starts from a straight annulus and then enters the coiled section. The negative shift due to inertial effect becomes maximum at the entrance of the coiled section. Around the entrance of the coiled section, the centrifugal force felt by the fluid particles in the core region is larger in this case than in the uniform inlet case because the streamwise velocity in the core region is considerably larger than the uniform average streamwise velocity. Thus, the recovery from the negative shift is very rapid in this case. When the flow starts from the uniform velocity at the entrance of the coiled section, the flow development is a little different. As seen from the curve for $\alpha = 0.2$ with uniform inlet velocity condition, the negative shift at the initial stage is very small and the recovery to the asymptotic state is very gradual. The very small amount of negative shift and the gradual recovery are obviously the results of the enforcement of the uniform velocity at the entrance. For both cases, however, the asymptotic values of M_o are nearly the same.

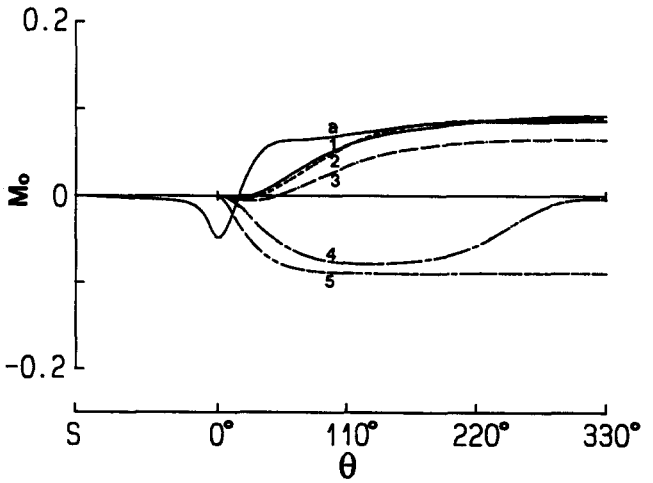

Figure 13 First moment of streamwise velocity; (a) ———, $\alpha = 0.2$, $\kappa = 640$; parabolic entry profile: (1) ———, $\alpha = 0.2$, $\kappa = 640$; (2) – – – –, $\alpha = 0.5$, $\kappa = 506$; (3) ———, $\alpha = 0.6$, $\kappa = 452$; (4) – · – · –, $\alpha = 0.8$, $\kappa = 320$; (5) – · · – · · –, $\alpha = 0.9$, $\kappa = 226$: uniform entry profile

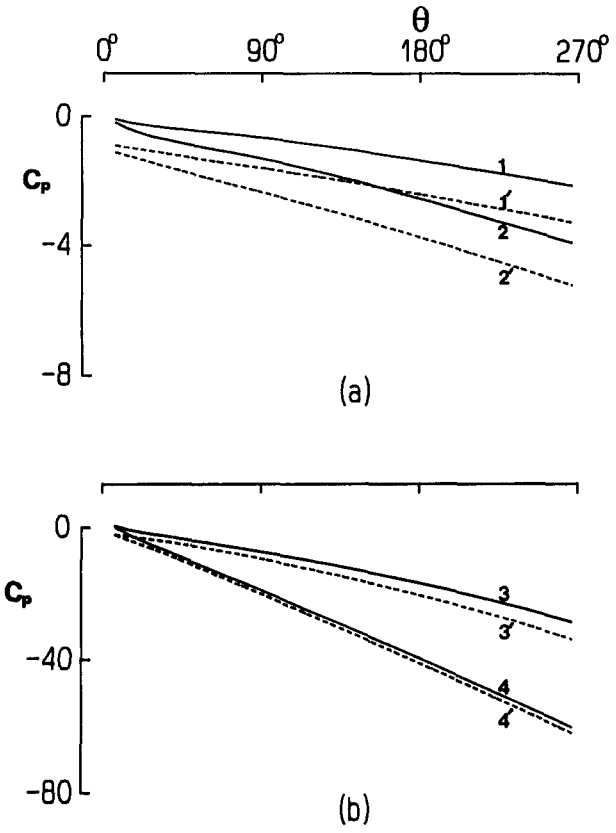

Figure 14 Streamwise pressure distribution along the inside bend ($\phi = 180°$, $r = 1$) and the outside bend ($\phi = 0°$, $r = 1$): ———, $\phi = 0°, r = 1$; – – – –, $\phi = 180°, r = 1$: (1), (1'), $\alpha = 0.2$; (2), (2'), $\alpha = 0.5$; (3), (3'), $\alpha = 0.8$; (4), (4'), $\alpha = 0.9$

The streamwise pressure distributions for several cases along the inside bend ($\phi = 180°$) and the outside bend ($\phi = 0°$) of the outer pipe ($r = 1$) are shown in Figure 14. It is seen that the streamwise pressure drop is nearly uniform for all the cases. However, when the radius ratio is large, the pressure drops very rapidly. The streamwise pressure drop for the cases of large radius ratio (Figure 14b) is greater by an order of magnitude than that for the cases of small radius ratio (Figure 14a). We also note that the percent difference between the inside bend pressure and the outside bend pressure gets smaller as the radius ratio increases. We expect that the pressure difference may become zero as the radius ratio approaches unity as would be the case of a straight annular duct.

Concluding remarks

Developing laminar flows in coiled annular ducts have been studied numerically by solving the full Navier-Stokes equation. Special attention has been given to the effect of radius ratio on the flow development. When the radius ratio is small, as has been previously found by Humphrey,[5] the secondary flow pattern is typified by a pair of counter-rotating vortices in the half cross section above or below the line of symmetry. The two-cell pattern results from the inward motion (i.e., in the direction of decreasing radius of curvature) along the inner and outer wall boundaries and the outward centrifugal motion (i.e., in the direction of increasing radius of curvature) in the core region. The strength and the position of these vortices are found to depend on the radius ratio. When the radius ratio becomes very large, however, the two-cell pattern breaks down and the secondary flow development is dominated by the inward motion, owing to the strong viscous action arising from the narrow gap. The extent of the central core region naturally diminishes with the increase of the radius ratio. The relative importance of the outward centrifugal motion over the inward motion may be judged by the centroid of the first moment of the streamwise velocity. When the radius ratio is moderate (say, smaller than 0.7), the centroid is found to lie on the outside half plane, implying the dominance of the outward centrifugal motion. When the radius ratio is very large (say, greater than 0.8), the centroid is seen to lie on the inside half plane owing to the influence of the strong inward motion.

Acknowledgments

Discussions with Professor J. M. Hyun of Korea Advanced Institute of Science and Technology and his continued interest during the course of this work are deeply appreciated. Constructive and valuable criticism offered by anonymous referees is also appreciated.

References

1 Berger, S. A., Talbot, L. and Yao, L. S. Flow in curved pipes. *Ann. Rev. Fluid Mech.*, 1983, **15**, 461–512

2 Lundgren, T. S., Sparrow, T. S. and Starr, J. B. Pressure drop due to the entrance region in ducts of arbitrary cross section. *Trans. ASME, J. Basic Eng.*, 1964, **86**, 621–626

3 Sparrow, E. M. and Lin, S. H. The developing laminar flow and pressure drop in the entrance region of annular ducts. *Trans. ASME, J. Basic. Eng.*, 1964, **86**, 827–834

4 McComas, S. T. Hydrodynamic entrance lengths for ducts of arbitrary cross section. *Trans. ASME, J. Basic Eng.*, 1967, **89**, 847–850

5 Humphrey, J. A. C. Numerical calculation of developing laminar flow in pipes of arbitrary curvature radius. *Canadian J. Chem. Eng.*, 1978, **56**, 151–164

6 Garimella, S., Richards, D. E. and Christensen, R. N. Experimental investigation of heat transfer in coiled annular ducts. *Trans. ASME, J. Heat Transfer*, 1988, **110**, 329–336

7 Chen, Y. S. A computer code for three-dimensional incompressible flow using nonorthogonal body-fitted coordinate system. *NASA* CR-178818, 1986

8 Hoffmann, K. A. Computational fluid dynamics for engineers. Engineering Education System, Austin, TX, 1989

9 Vanka, S. R., Chen, B. C. J. and Sha, W. T. A semi-implicit calculation procedure for flows described in boundary-fitted coordinates systems. *Numerical Heat Transfer*, 1980, **3**, 1–19

10 Patankar, S. V. *Numerical Heat Transfer and Fluid Flow*. McGraw-Hill, New York, 1980

11 Van Doomal, J. P. and Raithby, G. D. Enhancements of the SIMPLE method for predicting incompressible fluid flows. *Numerical Heat Transfer*, 1984, **7**, 147–163

12 Hille, P. and Vehrenkamp, R. The development and structure of primary and secondary flow in a curved square duct. *J. Fluid Mech.*, 1985, **151**, 219–241

13 Agrawal, Y., Talbot, L. and Gong, K. Laser anemometer study of flow development in curved circular pipes. *J. Fluid Mech.*, 1978, **85**, 497–518

14 Soh, W. Y. and Berger, S. A. Laminar entrance flow in a curved pipe. *J. Fluid Mech.*, 1984, **148**, 109–135

15 Humphrey, J. A. C., Whitelaw, J. H. and Yee, G. Turbulent flow in a square duct with strong curvature. *J. Fluid Mech.*, 1981, **103**, 443–463
16 Olson, D. E. and Snyder, B. The upstream scale of flow development in curved circular pipes. *J. Fluid Mech.*, 1985, **150**, 139–158
17 Futagami, K. Laminar heat transfer in a helically coiled tube. *Int. J. Heat Mass Transfer*, 1988, **31**, 387–396
18 Prusa, J. and Yao, L. S. Numerical solution for fully developed flow in heated curved tubes. *J. Fluid Mech.*, 1982, **123**, 503–522
19 Dennis, S. C. R. Calculation of the steady flow through a curved tube using a new finite-difference method. *J. Fluid Mech.*, 1980, **99**, 449–467
20 Zapryanov, Z., Christov, C. H. and Toshev, E. Fully developed laminar flow and heat transfer in curved tubes. *Int. J. Heat Mass Transfer*, 1980, **23**, 837–880
21 Soh, W. Y. and Berger, S. A. Fully developed flow in a curved pipe of arbitrary curvature ratio. *Int. J. Numerical Methods in Fluids*, 1987, **7**, 733–755
22 Bovendeerd, P. H. M., van Steenhoven, A. A., Yan De Vosse, F. N. and Vossers, G. Steady entry flow in a curved pipe. *J. Fluid Mech.*, 1987, **177**, 233–246